Bio-Design and Manufacturing (2022) 5:333–347
https://doi.org/10.1007/s42242-021-00174-z

RESEARCH ARTICLE

Structural optimization of patient-specific temporomandibular joint replacement implants for additive manufacturing: novel metrics for safety evaluation and biomechanical performance

Manuel Pinheiro[1] · Anouar Krairi[2] · Robin Willaert[3,4] · Maria C. Costa[1] · Wim Van Paepegem[1]

Received: 17 August 2021 / Accepted: 24 October 2021 / Published online: 27 January 2022

Abstract

Total temporomandibular joint (TMJ) replacement is recommended only when there is irreversible damage to the joint and no conservative treatment can provide functional improvements. Several stock and custom-made TMJ implants have been made available; however, retrospective and comparative studies were unable to find significant differences between the two types of solutions. The introduction of additive manufacturing (AM) techniques in medical practice allows for a greater freedom of design and a higher degree of device customisation. The combination of AM with structural optimisation may streamline development and provide the key for fabricating biomechanically enhanced TMJ implants. In this study, structural optimisation techniques were applied to develop and numerically validate a patient-specific TMJ implant. The biomechanical behaviour of each intermediate TMJ design was assessed under four different nominal and maximum biting tasks using finite element analyses. In addition, a new set of metrics were proposed to compare each design regarding biomechanical performance and implant safety. The results suggest that 55–82% of the natural/intact strain patterns can be recovered with the finally selected TMJ implant. This represents an increase of 15% in biomechanical performance for incisor biting, 15% for right molar biting, 17% for left molar biting and a decrease of 2% for left group biting compared with the initial design. The results also suggest that load transfer at the proximal ramus reduces the implant's impact on the mandible's strain patterns. Finally, structural optimisation allows for a volume reduction of up to 44% with a minimum loss of implant safety and biomechanical performance.

✉ Manuel Pinheiro
manuel.dasilvapinheiro@ugent.be

[1] Mechanics of Materials and Structures (MMS), Ghent University, Ghent, Belgium

[2] Materials Innovation Institute (M2i), Delft, The Netherlands

[3] Department of Oral and Maxillofacial Surgery, University Hospitals Leuven, Leuven, Belgium

[4] Department of Head and Neck Surgery, Ghent University Hospital, Ghent, Belgium

Graphic abstract

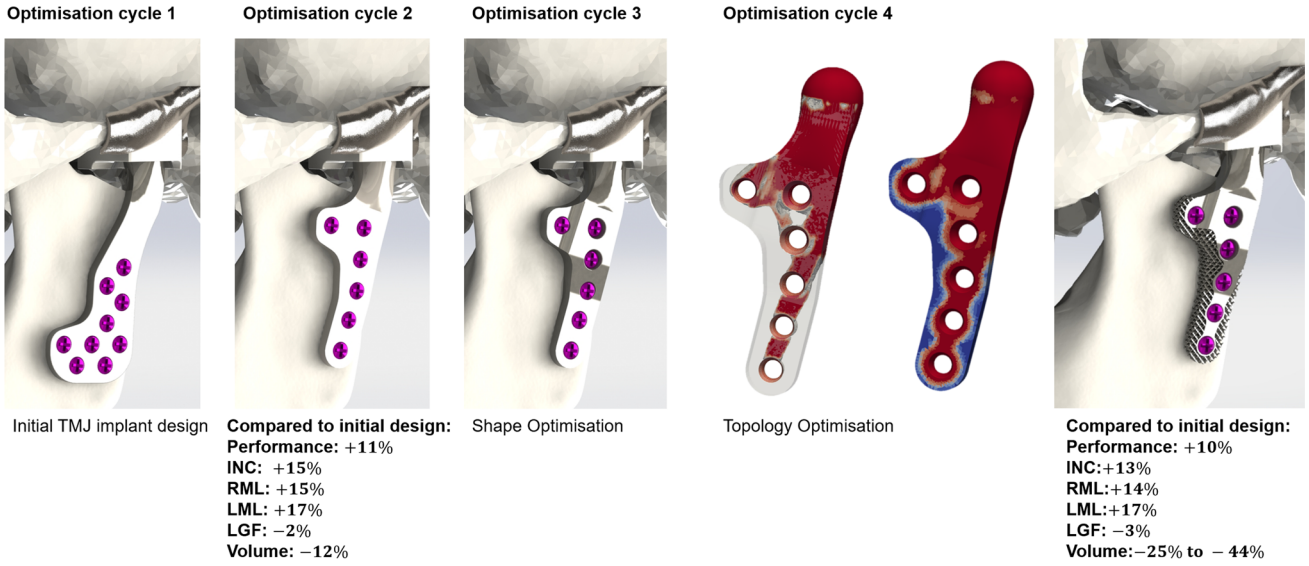

Keywords Temporomandibular joint · Additive manufacturing · Implant safety · Biomechanical performance · Finite element analysis

Introduction

Temporomandibular joint (TMJ) function can be impaired by multiple disorders, which can cause pain, decreased movement and disability, both regarding mouth opening, chewing, swallowing and speech. If irreversible damage to the joint is observed and all of the conservative treatments fail to produce functional improvements, the patient is recommended for alloplastic TMJ replacement [1, 2].

Currently, there are three stock TMJ replacement systems available, namely, the patient-fitted TMJ Concepts system (Ventura, CA, USA), the stock/custom Biomet Microfixation systems (Jacksonville, FL, USA) and the stock/patient-specific Nexus CMF systems (Salt Lake City, UT, USA). A meta-analysis comparing these designs showed no significant differences concerning the clinical outcomes [3]. All such designs show encouraging short-term results; however, their long-term success is still unclear [4]. One of the major disadvantages of stock prostheses is their limited ability to conform to a wide range of mandibular morphologies and bone pathologies [5].

Patient-specific and custom-fitted TMJ designs can adjust to the mandible with greater accuracy, allowing for shorter surgery times and more native tissue preservation [6]. Nevertheless, retrospective and comparative studies have failed to find significant differences between stock and custom-made implants [6, 7]. These observations, together with the time and financial costs associated with the manufacturing process [6], limit the application of these implants in the management of temporomandibular disorders. Custom-made TMJ implants are typically recommended in cases where (i) the stock implants do not fit, (ii) the TMJ is severely degenerated, (iii) there is an absent or deformed anatomical structure (e.g. in patients who have undergone multiple operations) and (iv) the jaw is mal-positioned; or (v) there is a need to change the occlusion with jaw repositioning [7].

Additive manufacturing (AM) technologies allow the design of arbitrarily complex structures directly from feedstock materials [8]. AM has found a wide range of applications in the medical field, most notably in the creation of highly accurate anatomical models and the production of patient-specific implants and instruments [9]. This manufacturing approach also enables design engineers to take full advantage of structural optimisation techniques to streamline product development while ensuring compliance with functional needs. Nevertheless, the mechanical properties of AM-fabricated parts (AM parts) vary considerably with the manufacturing process settings and post-processing techniques [10]. Therefore, the knowledge concerning the AM process should be considered during the design phase.

Recently, several new patient-specific TMJ implants with different degrees of design customisation were proposed [5, 11–14]. However, the combination of implant customisation, AM and structural optimisation was not addressed in the studies above. Therefore, the main objectives of this study are the design of a new TMJ using SO techniques suitable for AM and the provision of a framework for custom TMJ implant design and evaluation. In addition, novel metrics for

the assessment of both implant safety and biomechanical performance are proposed. The implant safety is evaluated considering various loading conditions while taking into account the local principal stress ranges. Implant safety is summarised by a modified Soderberg safety factor. Given the nodal mean principal stress and principal stress amplitude, a Soderberg map is also proposed to quantify the minimum implant safety for different yield and fatigue strength values. Given a target material and AM process, design engineers can apply the Soderberg map to assess the feasibility of a specific implant geometry. The biomechanical performance is quantified through a strain similarity index, and computed via the cross-correlation between the intact and implanted principal strain distributions. The impact of structural optimisation is also evaluated by quantitatively estimating the biomechanical performance and implant safety of each intermediate design. The structural optimisation approach and the proposed metrics can be applied in the design and evaluation of other types of implants.

Materials and methods

Finite element meshing

The finite element model used in this study was developed and described in [15]. Finite element (FE) meshing was conducted using Materialise 3-Matic (14.0, Materialise Inc., Leuven, Belgium) and Abaqus CAE 2019 (Abaqus Inc., USA). FE analyses, topology and shape optimisation models, and post-processing were performed in Abaqus CAE 2019, Abaqus TOSCA (Abaqus Inc., USA) and Paraview 5.8.0 (Kitware, New York, USA), respectively. All simulations were carried out using an Intel Xeon Gold 6146, CPU 3.20 GHz machine with 256 GB RAM.

The finite element mesh was generated using quadratic tetrahedral elements (C3D10). The mesh sensitivity analysis showed convergence on the nodal displacements for a maximum surface element edge length of 0.50 mm [15, 16]. The final intact model contained 3,446,040 nodes and 2,448,785 elements.

Material properties

The mandible was modelled as a non-homogeneous, isotropic and linear elastic solid, where the material distribution was encoded by the CT numbers (Fig. 1b). The CT-based material assignment was performed in Materialise Mimics as described in the literature [15]. Table 1 provides a summary of the power laws and mechanical properties assigned to each tissue.

All of the remaining structures were modelled using homogeneous, isotropic and linear elastic material properties. Ti–6Al–4V was used for the TMJ implant, fixation screws and shell of the fossa component, whereas ultra-high molecular weight polyethylene (UHMWPE) was employed as the liner of the fossa component (Fig. 1c).

Musculoskeletal forces

Bergmann et al. suggested that the implant should be evaluated under average, high and extreme loads during the design phase [29, 30]. Following these guidelines, the TMJ implant was evaluated under biting tasks including four nominal and maximum bite forces, namely incisor (INC), left group (LGF), left molar (LML) and right molar (RML) biting [18].

Several biomechanical studies have shown that the bite forces depend on the type of ingested food and can range from 50 to 700N [31]. Herein, the maximum bite forces for INC, LGF, RML and LML were 570, 1336, 911 and 911 N, respectively, whereas the nominal forces were set as 50% of the maximum forces [15]. Therefore, the set of nominal bite forces ranged from 200 to 485N, whereas the maximum bite forces varied between 511 and 1336N.

The muscle activations for each loading case were defined as described in the musculoskeletal model proposed by Korioth et al. [18] (Fig. 1a). The muscle forces were then scaled uniformly until the target nominal or maximum bite force was measured at the dental arch. Table 2 lists the muscle force components during the maximum bite force for each clenching task. The LML muscles forces were obtained by mirroring the RML muscle activations.

Boundary conditions

The model was constrained at the superior surfaces of the two cranial sections in all directions (Fig. 1a), and biting was simulated by constraining the teeth in the Oz-direction [18].

In the intact model, the contact between the right and left cartilage was modelled as frictionless. The interaction between the TMJ cartilage and cranial component was modelled with a tie constraint. In the implanted model, the left lateral pterygoid muscle was removed from the musculoskeletal model, and the left masseter muscle was assumed to be fully functional [32]. The interaction between implant and liner was set as frictional ($\mu = 0.05$), while the interactions between screws and mandible, screws and implant, polymeric liner-fossa component and fossa component-left cranial component were modelled as tied constraints.

Implant safety and printability

Localised stress concentrations are often associated with the fatigue failure of AM parts. These stress concentrations may be due to excessive surface roughness or internal geometrical defects. Failure can occur under tension and/or compres-

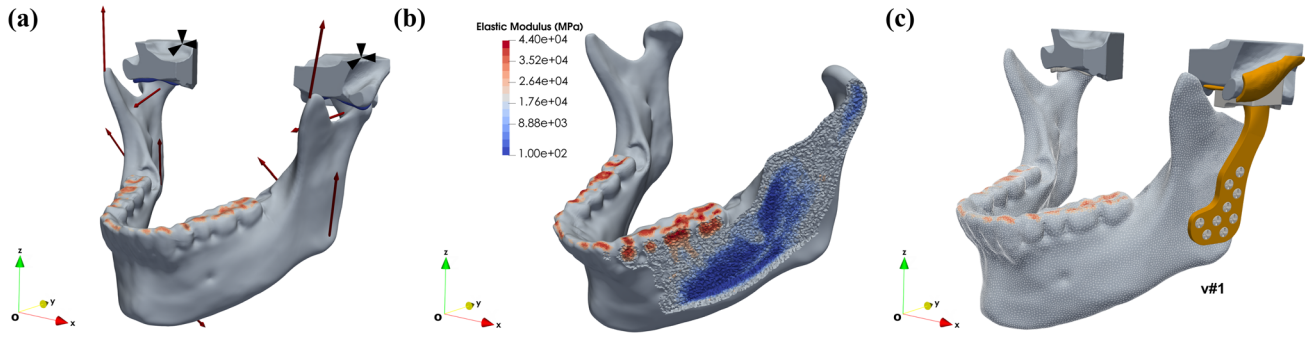

Fig. 1 Patient-specific model of the human mandible: **a** musculoskeletal model, **b** grayscale-based material distribution across the intact mandible and **c** implanted mandible for version v1

Table 1 Mechanical properties and power laws for the different materials considered in the finite element simulations

Tissue	Power law	Practical modulus (MPa)	Poisson's ratio (ν)	Yield strength (MPa)	Fatigue strength (MPa)	References
Trabecular bone	$E_T = 0.00040\rho_t^{P2.01}$	191 – 374	0.300	41 – 62	–	[15]
Cortical bone	$E_C = 0.0050\rho_c^{P2.01}$	7320 – 18140	0.300	140	–	[15, 17–20]
Dentin	$E_D = 0.0045\rho_d^{P2.01}$	21030 – 28040	0.300	–	–	[15, 21, 22]
Enamel	$E_E = 0.0050\rho_e^{P2.01}$	35230 – 43980	0.300	–	–	[15, 21, 22]
Ti–6Al–4 V	–	113800	0.342	664 – 1273	30 – 770	[19, 23–25]
Co–Cr	–	210000	0.290	448 – 841	207 – 950	[20–22]
UHMWPE	–	1258	0.460	20 – 30	13 – 20	[20, 26]
TMJ disc	–	15.8 – 65.0	0.400	–	–	[27, 28]

Table 2 Muscle forces for maximum incisor biting (INC), right molar (RML) and left group biting (LGF)

Muscle name	INC			RML			LGF		
	F_x (N)	F_y (N)	F_z (N)	F_x (N)	F_y (N)	F_z (N)	F_x (N)	F_y (N)	F_z (N)
Right masseter	– 121.82	– 108.35	371.57	– 96.61	– 58.21	264.87	– 99.19	– 62.27	274.64
Left masseter	121.82	– 108.35	371.57	80.51	– 48.51	220.72	103.24	– 17.18	234.61
Right temporalis	– 16.87	21.82	83.41	– 64.69	103.31	300.35	– 17.25	27.95	79.81
Left temporalis	16.87	21.82	83.41	54.36	85.06	252.75	173.53	295.08	787.71
Right lat. pterygoid	181.93	– 201.39	– 32.09	20.21	– 24.28	– 5.58	34.13	– 38.25	– 6.51
Left lat. pterygoid	– 181.93	– 201.39	– 32.09	– 43.78	– 52.61	– 12.09	– 130.48	– 149.89	– 28.76
Right med. pterygoid	295.05	– 226.45	480.22	114.00	– 87.50	185.55	288.07	– 221.09	468.85
Left med. pterygoid	– 295.05	– 226.45	480.22	– 81.43	– 62.50	132.54	– 26.53	– 20.36	43.18
Right ant. digastric	– 21.75	83.78	– 21.12	–	–	–	– 16.56	63.80	– 16.09
Left ant. digastric	21.75	83.78	– 21.12	–	–	–	22.23	85.63	– 21.59

sion, especially when lattice structures are applied in less mechanically demanding regions [10, 33, 34]. Furthermore, the compressive stiffness of an AM part can be dependent on the build orientation and strain rate [35].

Here, concepts related to fatigue under variable loading were redefined to take into account the likelihood for tensile and/or compressive failure of AM parts. The principal stress range $\sigma_r = |\sigma_I - \sigma_{III}|$ was defined as the primary design variable to be minimised. Therefore, σ_r should be maintained below the endurance limit of 3D-printed Ti–6Al–4V to guarantee implant safety. The value of σ_r was computed for each element considering the maximum principal tensile (σ_I) and compressive (σ_{III}) stresses across all loading cases.

To assess the fatigue life of the implant under variable loading conditions, the local Soderberg safety factor (S_f) [36] was calculated for every element considering both the first and third principal stresses $\{\sigma_I, \sigma_{III}\}$ according to the following formula:

$$S_f = \frac{1}{\frac{\sigma_a}{\sigma_f} + \frac{\sigma_m}{\sigma_y}}, \tag{1}$$

where $\sigma_a = \left|\frac{\sigma_I - \sigma_{III}}{2}\right|$ denotes the stress amplitude and $\sigma_m = \frac{\sigma_I + \sigma_{III}}{2}$ denotes the mean stress. S_f encapsulates the most extreme (local) tensile and compressive stimuli across the four loading cases in a scalar value.

The fatigue endurance limit (σ_f) and yield stress (σ_y) for 3D-printed Ti–6Al–4V can be set to represent a specific AM process. Similarly, after knowing σ_a and σ_m, a Soderberg safety factor map can be computed by varying σ_f and σ_y. Given a specific AM process, the Soderberg map can be used to assess the feasibility of a particular implant geometry. The minimum theoretical AM process requirements to safely produce each TMJ implant geometry were identified using the Soderberg map. The localised S_f values and Soderberg maps were computed for cases of both maximum and nominal load.

Biomechanical performance

The biomechanical performance of each implant design was assessed by comparing the principal strain distributions of intact versus implanted mandibles. The principal strain distributions (ε_{psd}) were computed as follows:

$$\varepsilon_{psd} = \begin{cases} \varepsilon_I, & \text{if } |\varepsilon_I| \geq |\varepsilon_{III}|, \\ \varepsilon_{III}, & \text{if } |\varepsilon_I| < |\varepsilon_{III}|, \end{cases} \tag{2}$$

where ε_I represents the first principal strain and ε_{III} represents the third principal strain ($\varepsilon_{III} \leq \varepsilon_{II} \leq \varepsilon_I$). The principal strain distribution along the intact mandible is denoted as $\varepsilon_{psd}^{intact}$, whereas the implanted mandible is denoted as $\varepsilon_{psd}^{implant}$ [15]. Since the FE meshes of the intact and implanted mandibles are inherently different, the principal strain distribution $\varepsilon_{psd}^{intact}$ was interpolated onto the nodes of the implanted mandible ($\hat{\varepsilon}_{psd}^{intact}$). This mapping technique not only allows for a node-to-node comparison between the two distributions, but also the computation of the overall biomechanical performance of the implant via normalised cross-correlation (α) between $\hat{\varepsilon}_{psd}^{intact}$ and $\varepsilon_{psd}^{implant}$:

$$\alpha = \frac{\hat{\varepsilon}_{psd}^{intact} \varepsilon_{psd}^{implant}}{\sqrt{\left(\hat{\varepsilon}_{psd}^{intact}\right)^2 \left(\varepsilon_{psd}^{implant}\right)^2}}. \tag{3}$$

The computation of α, as proposed here, provides a summarised and convenient measure of the similarity between the two principal strain distributions.

Implant design workflow

In order to guarantee the anatomical alignment of the TMJ implant, the 3D model was positioned in the natural head position by computing the cranial symmetry and defining the McNamara line as the true vertical direction [37]. The anatomical model was then exported in stereolithography (STL) format, and the implant design was created in SolidWorks (Dassault Systems, 2018).

The initial patient-specific TMJ design was based on the Biomet Microfixation systems design and fitted to the patient by (i) customising the proximal curvature to recover the original joint centre of rotation, (ii) adjusting the implant length to the size of the ramus and (iii) positioning the fixation screws such that the mandibular nerve is avoided (Fig. 1c). The TMJ implant was modelled to behave as a purely rotational joint, and the screw diameter was set to 2.7 mm for all designs.

Figure 2 shows the evolution of the TMJ implant design over different design cycles. Each design cycle was divided into three steps:

1. *CAD modelling*: design, redesign or post-processing of the structural optimisation results;
2. *Biomechanical evaluation*: maximum and nominal INC, LGF, RML and LML biting;
    a. Computation of the critically loaded areas (σ_r) and implant safety factors S_f; and
    b. Comparison of the principal strain patterns (α).
3. *Structural optimisation cycle*:
    a. Topology optimisation (TO): computation of the optimal material distribution; or
    b. Shape optimisation (SO): reduction of localised stress by changing the local thickness.

Both TO and SO were used interchangeably to tackle the current design needs. For instance, in design cycle 1, the results of TO were used as an additional guideline for implant redesign, whereas in design cycle 2, SO was used to locally adapt the implant thickness to the surface stress fields (Fig. 2).

Topology and shape optimisation

Structural optimisation is a powerful design tool; however, it has high computational demand. The extensive Abaqus wall clock time for full FE model simulation makes structural optimisation impractical. Therefore, the following simplifications were implemented:

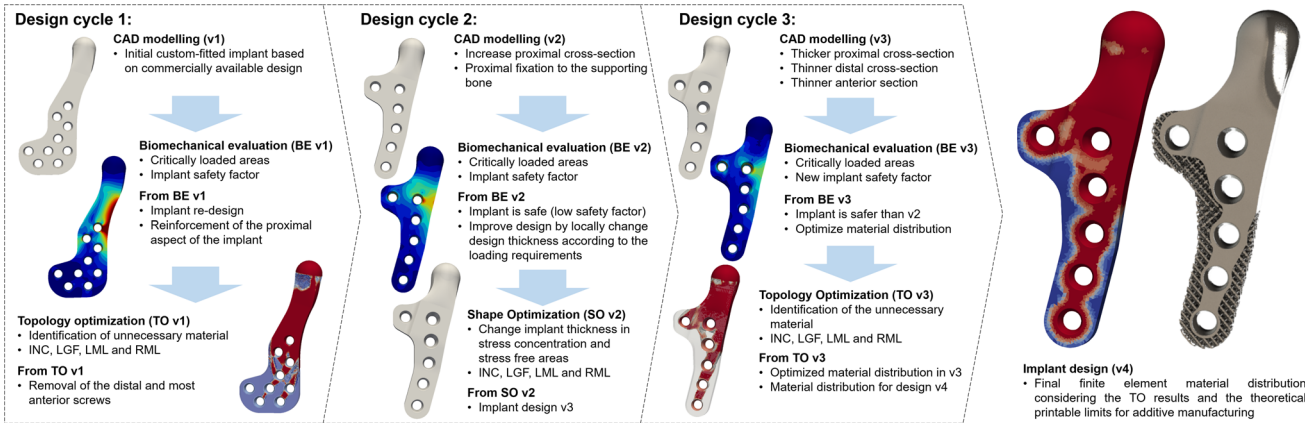

Fig. 2 Implant design and optimisation workflow: each design cycle was comprised of a biomechanical evaluation step and a design optimisation step, where the implant design was subjected to topology or shape optimisation (e.g., in design cycle 2, shape optimisation was applied to implant v2 instead of topology optimisation to generate implant v3)

1. Replace the screws with beam elements (Fig. S1);
2. Replace C3D10 with linear tetrahedral elements (C3D4) in the mandible;
3. Replace the condylar fossa with reference points;
4. Apply the average condylar displacements obtained from the full model to the reference points to mimic the original boundary conditions.

The interactions between the reference points and the corresponding surfaces at the implant and mandible side were set as tied. These simplifications allowed for a significant reduction (99.6%) of the computation time to approximately 4 min. per iteration. For completion, the differences in nodal displacements between the full and the simplified models are presented in Fig. S1b.

Topology optimisation (TO) was applied to minimise the strain energy density (C) while reducing the volume of the implant:

$$\min_{\boldsymbol{\rho}} C(\boldsymbol{\rho}, \boldsymbol{U}) = \boldsymbol{F}^{\mathrm{T}}\boldsymbol{U}$$
$$\text{s.t.} \begin{cases} \boldsymbol{K}\boldsymbol{U} = \boldsymbol{F}, \\ \frac{V(\boldsymbol{\rho})}{V_0} \leq 0.50, \\ 0 < \rho_{\min} < \rho_i < 1.0, \end{cases} \tag{4}$$

where $\boldsymbol{\rho}$ represents the set of normalised material densities, $\boldsymbol{U}$ represents the vector of virtual displacement, $\boldsymbol{K}$ represents the global stiffness matrix, and $\boldsymbol{F}$ is the body force vector [38]. TO was conducted over 30 iterations and for all cases with maximum load. In implant v4, the final normalised densities were computed considering a minimum printable normalised density of $\rho_{\min} = 0.075$ [39] and a minimum local safety factor of $S_{\mathrm{f}} \geq 2.0$.

Shape optimisation (SO) aims to adapt the mesh to the local surface stress levels. Mesh adaptation is accomplished by displacing the mesh nodes inwards or outwards depending on the local stress levels and a predefined stress threshold (σ_{ref}). In Abaqus TOSCA, the SO problem is formulated as a minimisation of the maximum design response:

$$\min_{\Gamma} \max \left| \sigma_k\left(\Gamma^*\right) - \sigma_{\mathrm{ref}} \right| \quad \Gamma^* \in \Gamma. \tag{5}$$

In TOSCA, σ_{ref} is by default set as the average objective value in the design nodes Γ^*, which belong to the entire boundary Γ of the domain, and σ_k is the stress measure at load case k [40]. In SO, $\sigma_{\mathrm{ref}} = \sigma_{\mathrm{f}}$ and the design boundary is set as the anterior, posterior and lateral surfaces of the implant and below the condylar surface.

Results

Displacement of implanted mandible across the implant designs

Figures 3a–3d show the nodal displacements along the distal contour of the intact and implanted mandibles (v1 to v4) during nominal and maximum INC biting. For maximum INC biting, the implanted mandible shows a greater upward movement of the right condyle (Fig. 3b), together with compression of the gonial area and lateral deviation towards the right side (Fig. 3c). The forward movement of the mandible is also increased when compared with the intact model (Fig. 3d). The mediolateral deviation and anteroposterior movement are decreased for v2–v4 when compared to implant v1.

In LGF, the implanted mandible moves downwards on the healthy side and at the implanted side (Fig. S2a). It also moves towards the implanted (left) side and posteriorly (Figs. S2b

and S2c). Slightly higher displacements were observed for implant v1 compared to implants v2–v4. In LML and RML, a slight downward movement of the balancing condyle, as well as a mediolateral displacement towards the right side was observed (Figs. S3a, S3b, S4a, and S4b). The forward movement is more noticeable during LML than RML (Figs. S3c and S4c). No other displacement differences were observed across the different designs.

Principal stress range and Soderberg safety factors

The principal stress range (σ_r) and the Soderberg safety factor (S_f) were computed across the entire geometry for both the maximum and the nominal bite forces (Figs. 4 and S5). Here, the S_f values were computed for the minimum $\sigma_f = 450$ MPa reported in the literature [23] and the typical $\sigma_y = 880$ MPa for Ti–6Al–4V (Table 1). In implant v1, the maximum σ_r was found around the outer posterior (562 MPa) and medial anterior (540 MPa) surfaces of the implant and around the first proximal screw (661 MPa) (Fig. 4a). For the maximum bite forces, the minimum S_f was approximately 1.47 around the first proximal screw (Fig. 4b), while for nominal forces, the minimum S_f was about 3.00 (Fig. 4c).

Similarly, the main critical areas in implant v2 were around the first screw [$\sigma_r = 369$ MPa, minimum $S_f = 1.91$ (Figs. 4d and 4e)] and the anterior surface of the neck of the implant ($\sigma_r = 465$ MPa, Fig. 4d). For nominal loads, a minimum $S_f = 3.99$ was observed around the first screw (Fig. 4f). For implant v3, the maximum principal stress ranges were $\sigma_r = 290$ MPa ($S_f = 2.43$) around the first screw, $\sigma_r = 226$MPa in the posterior surface ($S_f = 3.29$) and $\sigma_r = 341$ MPa along the anterior surface ($S_f = 3.43$). Meanwhile, in implant v4, the maximum σ_r was slightly higher than that in implant v3 ($\sigma_r = 362$ MPa, Fig. 4g). A minimum $S_f = 2.39$ was obtained for the maximum loads (Fig. 4h), whereas $S_f = 4.94$ was obtained for nominal loads (Fig. 4i).

The mechanical properties of AM parts may vary considerably due to a multitude of manufacturing parameters. From a product development perspective, it may be relevant to assess the design safety and feasibility, given the prior knowledge of the fatigue and endurance limits of a particular AM process. The variation of the minimum design S_f across all combinations of σ_y and σ_f for AM Ti–6Al–4V described in Table 1 are plotted in the newly proposed Soderberg safety factor maps. From these maps, it can be observed that, for implant v1, $S_f \geq 2.0$ can be obtained for $\sigma_f \geq 600$ MPa and $\sigma_f \geq 400$ MPa for the maximum and the nominal bite forces, respectively (Figs. 5a and 5b). For implant v4, $S_f \geq 2.0$ can be theoretically obtained for $\sigma_f \geq 300$ MPa, but only if $\sigma_y \approx 1200$MPa under the maximum bite force (Fig. 5c). For nominal bite forces, $S_f \geq 2.0$ can be theoretically obtained for $\sigma_f \geq 200$ MPa (Fig. 5d).

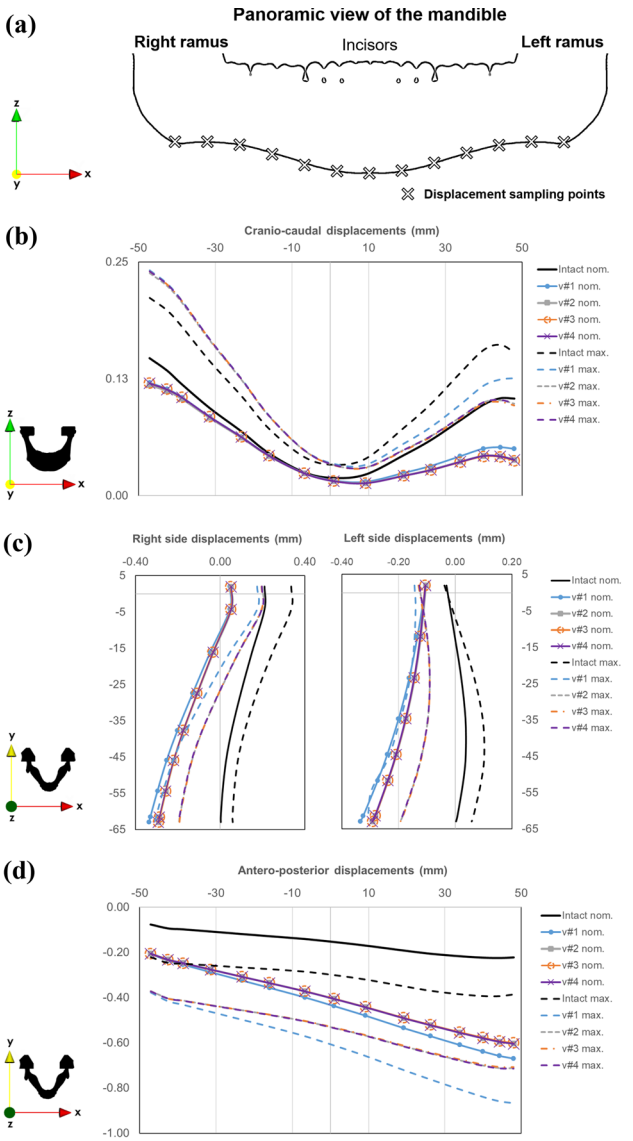

Fig. 3 Displacements along the lower contour of intact and implanted mandibles (designs v1 to v4) during nominal and maximum INC biting: **a** panoramic view of the mandible and displacement sampling points; **b** craniocaudal (Oz) displacements; **c** mediolateral (Ox) displacements (middle); **d** anteroposterior (Oy) displacements

Biomechanical performance

The principal strains observed in the intact mandible during the maximum INC have an average value of $\bar{\varepsilon} = -61.62\mu\varepsilon$ (with a standard deviation $s_\varepsilon = 869.16\mu\varepsilon$) (Fig. 6a). The peak compressive strains ($-3000\mu\varepsilon$) occurred along the posterior aspect of the rami, whereas the maximum tensile strains ($3000\mu\varepsilon$) were observed around the mandibular notch. In implant v1, the mean principal strain values were $-254.03\mu\varepsilon$ ($s_\varepsilon = 1227.80\mu\varepsilon$) (Fig. 6b). For implants v2–v4, the principal strain values were closer to

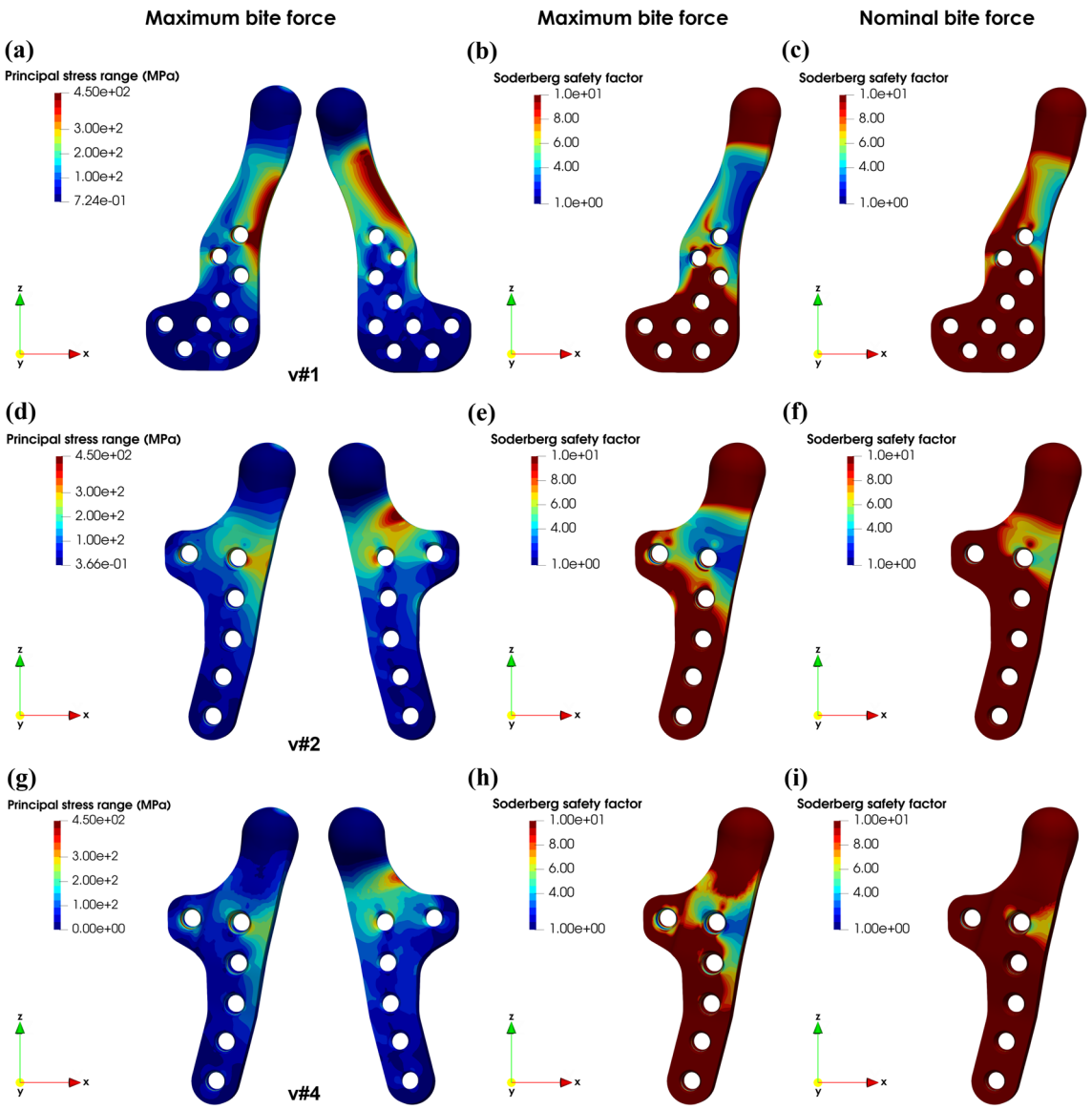

Fig. 4 Biomechanical evaluation of the TMJ design: **a** principal stress range and **b** Soderberg safety factor for maximum bite forces, **c** Soderberg safety factor for nominal bite forces across implant v1; **d** principal stress range and **e** Soderberg safety factor for maximum bite forces, **f** Soderberg safety factor for nominal bite forces across implant v2; **g** principal stress range and **h** Soderberg safety factor for maximum bite forces, **i** Soderberg safety factor for nominal bite forces across implant v4 ($\sigma_f = 450$ MPa and $\sigma_y = 880$ MPa)

those observed in the intact mandible ($\overline{\varepsilon} = -180\mu\varepsilon$) when compared with implant v1 (Figs. 6c and 6d; Table 3).

Table 3 presents the average and standard deviations of the principal strain distributions for all implant designs across all values of maximum and nominal bite forces. The main improvements in principal strain distribution (ε_{psd}) were observed when changing from implant v1 to implant v2. Meanwhile, no significant improvements were observed between implant v3 and v4. These observations were more evident when comparing the cross-correlation (α) between the intact and implanted mandibles for all types of design (Table 4). When switching from implant v1 to v2, α increases for INC (+15%), RML (+15%), LML (+17%) and decreases slightly for LGF (−2%). For designs v3 and v4, the strain patterns as well as α remain relatively unchanged.

Figures 7a–7l show the principal strain distributions (ε_{psd}) at the lateral surface of the ramus for the intact and implanted mandibles during maximum INC, LGF and RML biting. The main differences between intact and implanted mandibles were observed in the implanted ramus around the screws, especially around the most proximal and most distal screws.

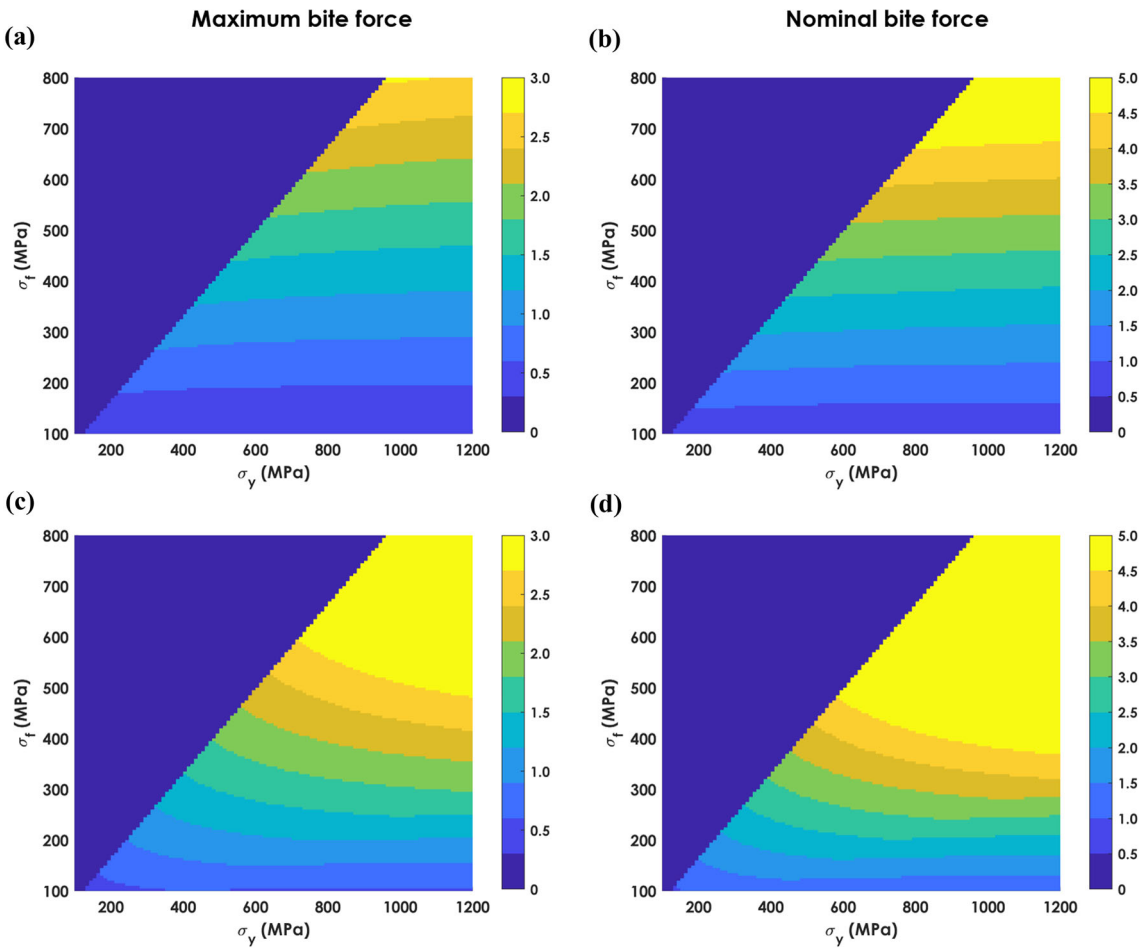

Fig. 5 Minimum Soderberg safety factors for different combinations of yield stress (σ_y) and fatigue (σ_f) stress values for implant v1 under **a** maximum and **b** nominal bite forces; for implant v4 under **c** maximum and **d** nominal bite forces

Discussion

Temporomandibular joint (TMJ) function can be affected by multiple disorders. Current TMJ replacement systems have limited applications. Furthermore, retrospective and comparative analyses have failed to justify the use of patient-specific designs instead of stock prostheses in the management of temporomandibular abnormalities. The combination of AM with structural optimisation techniques allows for a higher level of implant customisation by adjusting the design to localised biomechanical demands. However, recent developments in patient-specific TMJ replacement designs have not addressed the synergetic combination of these manufacturing and design techniques [5, 11–14]. Here, a combination of patient-specific design and structural optimisation was used to develop a TMJ implant with improved biomechanical performance that is suitable for AM. Furthermore, metrics for implant evaluation concerning safety and biomechanical performance were also proposed. The behaviour of intact and implanted mandibles was compared considering both displacements and principal strain patterns.

The intact mandible can undergo largely different displacement patterns during mastication. The displacements obtained in this work are consistent with the patterns observed in Korioth et al. [18] (for more details, refer to [15]). Regarding the implanted mandible, the craniocaudal, mediolateral and anteroposterior displacements are consistent across different implant designs. The mediolateral and anteroposterior displacements are also larger for the implanted mandible than the intact mandible. In INC and LGF, the implants v2–v4 present less mediolateral and anteroposterior displacements when compared with the initial design, and they seem to provide a more natural displacement of the mandible.

The principal strain values along the intact and implanted mandible for both the maximum and the nominal bite forces are within the physiological values. The typical peak physiological strains in adult load-bearing bones can range from

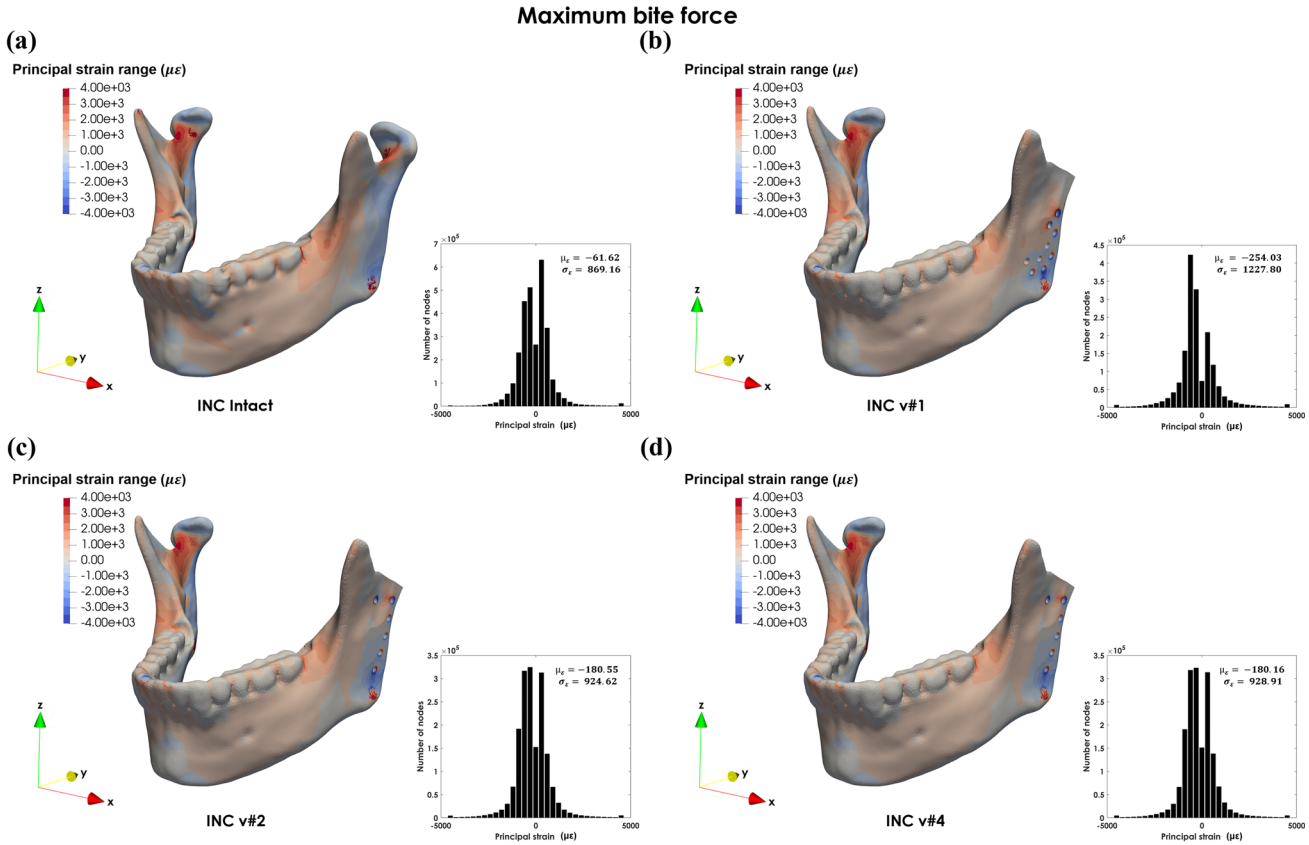

Fig. 6 Principal strain distribution under maximum INC bite forces for the **a** intact mandible, **b** implant v1, **c** implant v2 and **d** implant v4

Table 3 Mean and standard deviation of principal strain distributions ($\overline{\varepsilon}(s_\varepsilon)$) for maximum and nominal bite forces and the intact mandible and implant designs v1, v2, v3 and v4

Model	INC		LGF		LML		RML	
	Max	Nom	Max	Nom	Max	Nom	Max	Nom
Intact	− 61.62 (869.16)	− 34.98 (460.27)	− 32.09 (896.30)	− 22.64 (460.04)	− 17.55 (520.64)	− 10.56 (259.67)	− 4.03 (532.28)	− 2.16 (273.93)
Implant v#1	− 254.03 (1227.80)	− 127.95 (613.91)	− 286.04 (1124.10)	− 148.74 (583.60)	− 124.46 (477.98)	− 63.97 (241.32)	− 135.24 (527.94)	− 67.73 (263.45)
Implant v#2	− 180.55 (924.62)	− 91.34 (464.83)	− 305.12 (968.52)	− 157.93 (496.78)	− 109.09 (434.62)	− 55.80 (220.49)	− 113.57 (483.44)	− 56.69 (241.86)
Implant v#3	− 180.28 (924.53)	− 91.18 (464.71)	− 307.72 (971.27)	− 159.36 (498.39)	− 109.21 (435.35)	− 55.86 (220.93)	− 114.18 (485.43)	− 57.31 (242.64)
Implant v#4	− 180.16 (928.91)	− 91.18 (466.97)	− 306.32 (972.75)	− 158.60 (499.20)	− 109.43 (435.58)	− 55.97 (221.07)	− 114.16 (486.31)	− 57.30 (243.10)

2500$\mu\varepsilon$ in tension to 4000$\mu\varepsilon$ in compression [41]. In a FE study, Ichim et al. observed that strains ranged from 100 to 750$\mu\varepsilon$ during 552.6 N premolar biting and molar biting along the buccal and lingual surfaces of the mid-corpus. Maximum surface strains up to 1250$\mu\varepsilon$ were reported to occur in the alveolar area [42]. Gröning et al. reported principal strain values higher than $\pm$1500$\mu\varepsilon$ during incisal, canine and molar biting [43].

Herein, the principal strain values for the maximum bite forces were $\pm$3000$\mu\varepsilon$ during INC and they ranged from −3500 to 4500$\mu\varepsilon$ for LGF. During LML and RML biting, the principal strain values ranged from −2300 to 2000$\mu\varepsilon$. The maximum principal strain values were within the expected values taken from the literature. One exception occurred in LGF biting at the insertion of the left temporal muscle with a tensile strain of 4500$\mu\varepsilon$. However, the simulated bite force was extremely high (1336N) and very

Table 4 Cross-correlation between the principal strain distributions for maximum and nominal INC, LGF, LML and RML biting (higher α implies more similarity with the intact mandible)

Implant	α maximum bite force				α nominal bite force			
	INC	LGF	LML	RML	INC	LGF	LML	RML
v#1	0.4246	0.5333	0.6549	0.5399	0.4304	0.4892	0.6524	0.5357
v#2	0.5767	0.5141	0.8267	0.6931	0.5790	0.4693	0.8135	0.6716
v#3	0.5733	0.5062	0.8265	0.6915	0.5757	0.4620	0.8146	0.6679
v#4	0.5506	0.4967	0.8237	0.6843	0.5524	0.4543	0.8144	0.6613

close to the maximum non-pathological bite force of 1500N reported in the literature [44–46]. The maximum bite force in LGF can be used for the validation of the mechanical integrity of the implant; however, it may be too extreme for the mandible used in this study. For nominal bite forces, the maximum principal strain values were also observed during LGF biting at the insertion of the left temporal muscle. The maximum tensile strain was $2120\mu\varepsilon$, which was within the normal physiological range [15].

Regarding design safety, several biomechanical investigations have shown that standardised mechanical tests may not precisely reflect the critical biomechanical loads that an implant is subjected to during its life cycle. Bergmann et al. concluded that ISO standards underestimate real loading conditions, at least for patients with unfavourable anatomical and muscular conditions and high body weight [47]. The same author obtained similar results for total knee replacements [30]. For the development of implant design, safety factors of 1.115 [48] and 1.16 [49] have been reported using ISO protocols.

In this paper, a safety factor of 2.0 was set as the minimum acceptable value. Implant design v3 was the safest design, with a minimum safety factor of 2.43 and 5.06 for maximum and nominal bite forces, respectively. Furthermore, biomechanical studies have shown that the bite forces depend on the type of food that is ingested and can range from 50 to 700N [31]. Xu et al. observed that patients suffering from temporomandibular disorders present a reduction of maximum bite force of $41 \pm 20\%$ during unilateral premolar biting [50]. Therefore, the maximum bite forces considered here may represent extreme loads for all biting conditions in patients suffering from temporomandibular disorders.

Ackland et al. compared the biomechanical performance of a 3D-printed patient-specific Melbourne implant with that of a medium-size Biomet Microfixation TMJ implant under normal (200 N) and maximum (800 N) bilateral molar biting. The von Mises stresses in the Melbourne prosthetic ranged from 259.6 to 312.9 MPa, whereas in the Biomet Microfixation system, they ranged from 284.2 to 416.0 MPa under normal and maximum bite forces, respectively [5]. In a subsequent study, the patient-specific Melbourne design was patient-fitted and simulated under the same boundary conditions. The maximum von Mises stress reported was 105.0 MPa for the baseline design [51]. Considering a fatigue endurance limit $\sigma_f = 450$MPa and the reported stress levels, the Melbourne design provides a minimum safety factor of 4.28, which is considerably higher than the minimum $S_f = 2.39$ of implant v4. However, the maximum bite forces applied to the former were considerably lower than the forces used in the current study (especially for LGF). The maximum von Mises stress observed in implant v4 was approximately 286.5 MPa across all loading cases, which is comparable with the values obtained in the literatures [5, 51].

In order to carry out the biomechanical evaluation of the implant, the correlation coefficient (α) between the intact and implanted mandibles was computed. An increase in the correlation coefficient between strain patterns was observed with the change from implant v1 to v2, and it remained approximately constant across v3 and v4. These observations are in line with previous results by Mesnard et al., who suggested that, in order to reduce the strain shielding, it is important to transfer the load more proximally [52]. The values of α show that TMJ reconstruction only allows for the partial recovery of the original strain patterns ($0.42 < \alpha < 0.82$), even when considering a fully functional implanted side (except the lateral pterygoid muscle). For implants v2–v4, an average increase of approximately 10–11% in the biomechanical performance was observed for both nominal and maximum bite forces. However, a reduction in α may be observed if the muscular morbidity, that often accompanies TMJ degeneration, is also considered.

Mesnard et al. observed that the first and the last screws were the most critically loaded ones, and that the low strains at the third screw may lead to screw loosening [52]. In addition, Ackland et al. suggested that the condylar component thickness may influence the proportion of load transmitted to the fixation screws, and that the thickness should be chosen to distribute TMJ forces evenly across the fixation screws. It was also observed that decreasing the thickness of the condylar component increases the peak condylar and screw stresses, particularly in the screws closer to the TMJ articulation [51]. In the design v2 of this study, the peak reaction forces were observed at the two most proximal screws and at the most distal screw. SO was applied to adjust the design to the biomechanical demands while preserving the initial volume. The increase in thickness showed little impact on the reaction forces, which remained relatively unchanged in the designs v2–v4.

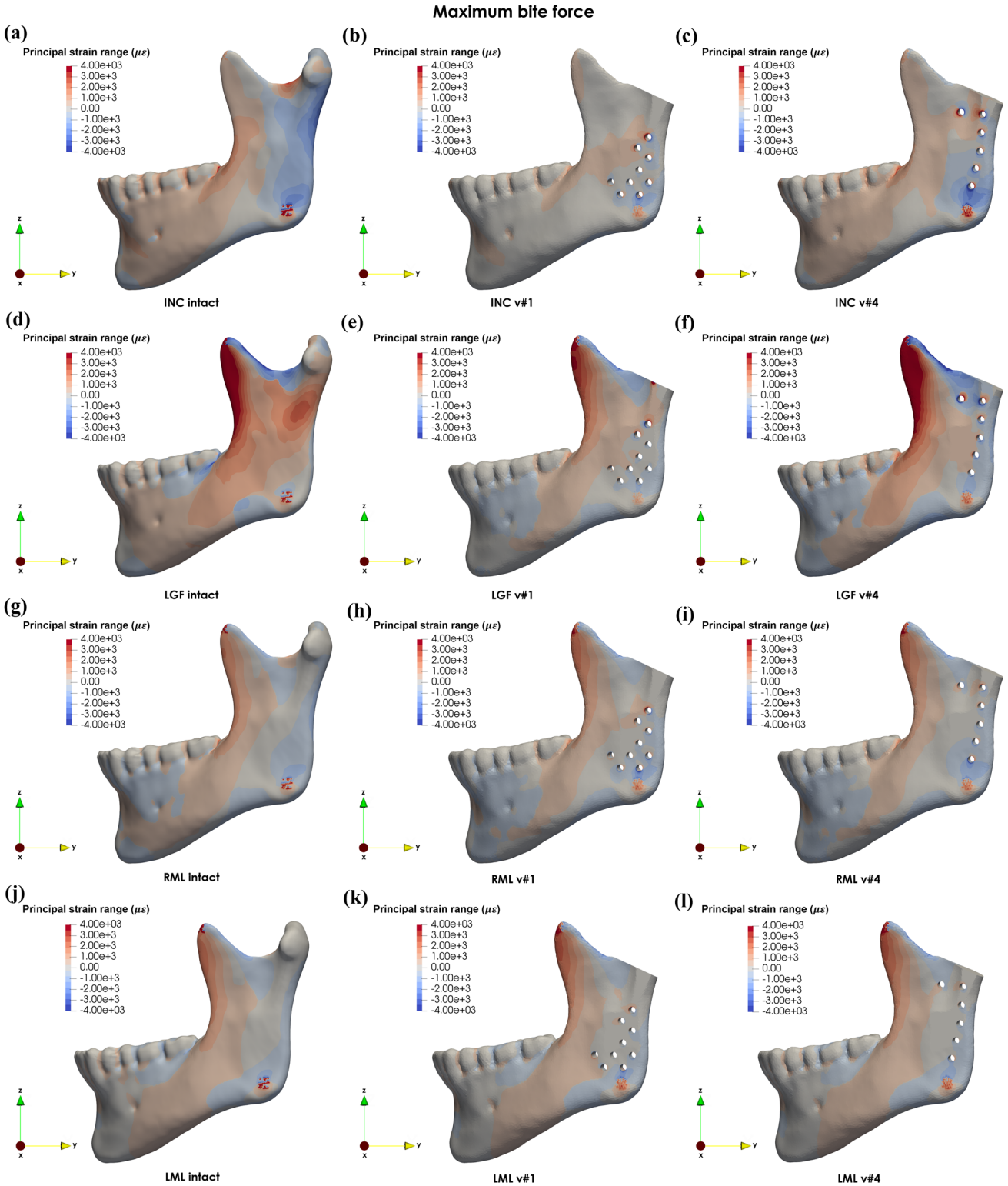

Fig. 7 Principal strain distributions (ε_{psd}) during maximum INC biting between the intact mandible **a** and implanted mandibles **b** v1 and **c** v4; for maximum LGF biting: **d** intact, **e** v1 and **f** v4; for maximum RML biting: **g** intact, **h** v1 and **i** v4, and for maximum LML biting: **j** intact, **k** v1 and **l** v4 (negative values indicate an inversion from tension to compression)

Concerning structural optimisation, Al-Tamimi et al. used TO to reduce the equivalent stiffness of the fixation plates in order to promote a more efficient load transfer between the implant and the supporting bone. The decrease in stress-shielding was mainly a consequence of the high percentage of volume reduction [53]. On the contrary, Guo et al. showed that TO could be used to improve patient-specific interspinous implants by allowing a better load distribution while providing a comparable amount of spinal stability [54]. Similarly, Iqbal et al. used multi-objective TO to obtain the appropriate material distribution of a pelvic prosthesis that fits all types of iliac bone resections. The implant was simultaneously optimised to different loading conditions, and it was both lightweight and safe [55]. In our study, TO and SO had a limited impact on α, which can be explained by the fact that load transmission is provided by the fixation screws. The obtained results correlate more with [53], i.e. TO contributions to volume reduction did not lead to optimised material distribution (and consequently a greater α).

For implant v3, the TO results show that a volume reduction of up to 44% can be obtained and that the two most distal screws can be removed from the design. This emphasises the importance of proximal load transmission in TMJ replacement. However, removing more screws may render a more unstable implant, since a minimum of 5 fixation screws is often recommended. Incorporating both TO and SO allowed for a theoretically safer and lighter design than the initial design. Nevertheless, additional investigations are needed to fully understand the long-term implications of the design changes proposed in this study and the clinical impact of TO and SO outputs in patient-specific TMJ implant designs. Furthermore, the incorporation of lattice structures in less mechanically demanding regions may allow the stimulation of bone ingrowth onto the implant and thus further improve its the implant biomechanical performance.

The main limitation of the current study is that implant optimisation was performed under maximum bite forces, which were set as the maximum forces in the literature for each task; these values may be considered extreme for patients with TMJ disorders. Although the optimisation of the fossa component was not considered in this study, it is important to note that high stresses were observed along the polymeric part of the fossa component for the current maximum bite forces (Fig. S6a). This indicates that the values used may be too high compared with the bite forces produced by patients with TMJ disorders. To the best of our knowledge, the biting capabilities of patients suffering from TMJ disorders are currently unknown. Therefore, a comprehensive evaluation of the range of bite forces generated by such patients is needed to further optimise the TMJ system. Under less demanding boundary conditions, a design with even better biomechanical performance may be feasible. Figures S6b and S6c, respectively, show the von Mises stresses (MPa) observed at the cranial shell and cranial base during maximum LGF. Based on these values, the risk of cranial base failure was not observed in the current study.

In summary, novel metrics for evaluating the safety and biomechanical performance of implants can help to predict both the theoretical feasibility and the biomechanical behaviour of such implants during the design phase. The final design allows for the recovery of 55–82% of the native principal strain patterns. In the present work, a performance increase of +15% in INC, +15% RML and +17% LML was observed as compared with the initial design, whereas a performance decrease of −2% in LGF was demonstrated. These improvements in biomechanical performance provide new insights into TMJ replacement design, which may lead to the development of implants with better long-term behaviour. In addition, a volume reduction of up to 44% can be obtained from the initial to the final design, depending on the normalised density value used to extract the TO results and the addition of lattice structures in less demanding areas. The application of the proposed metrics in the development of novel patient-specific implants will be a topic for future investigations.

Supplementary Information The online version contains supplementary material available at https://doi.org/10.1007/s42242-021-00174-z.

Acknowledgements This project has received funding from the Interreg 2 Seas program 2014–2020 co-funded by the European Regional Development Fund under subsidy contract no. 2S04-014.

Author contributions MP contributed to conceptualisation, formal analysis, software, investigation, methodology, visualisation and writing—original draft; AK contributed to software, formal analysis and writing—review and editing; RW contributed to resources and writing—review and editing; MCC contributed to writing—review and editing; WVP contributed to conceptualisation, methodology, supervision and writing—original draft.

Declarations

Conflict of interest The authors declare that they have no conflict of interest.

Ethical approval The anonymised CT dataset was provided with permission from the Ghent University Hospital institutional review board (B670201733474). All participants provided written informed consent allowing the information to be used for research purposes.

References

1. De Meurechy N, Mommaerts MY (2018) Alloplastic temporomandibular joint replacement systems: a systematic review of their history. Int J Oral Maxillofac Surg 47(6):743–754. https://doi.org/10.1016/j.ijom.2018.01.014
2. Wolford LM, Mercuri LG, Schneiderman ED et al (2015) Twenty-year follow-up study on a patient-fitted temporomandibular joint

prosthesis: The Techmedica/TMJ Concepts device. J Oral Maxillofac Surg 73(5):952–960. https://doi.org/10.1016/j.joms.2014.10.032
3. Zou L, He D, Ellis E (2018) A comparison of clinical follow-up of different total temporomandibular joint replacement prostheses: a systematic review and meta-analysis. J Oral Maxillofac Surg 76(2):294–303. https://doi.org/10.1016/j.joms.2017.08.022
4. Johnson NR, Roberts MJ, Doi SA et al (2017) Total temporomandibular joint replacement prostheses: a systematic review and bias-adjusted meta-analysis. Int J Oral Maxillofac Surg 46(1):86–92. https://doi.org/10.1016/j.ijom.2016.08.022
5. Ackland DC, Robinson D, Redhead M et al (2017) A personalized 3D-printed prosthetic joint replacement for the human temporomandibular joint: from implant design to implantation. J Mech Behav Biomed Mater 69:404–411. https://doi.org/10.1016/j.jmbbm.2017.01.048
6. Siegmund BJ, Winter K, Meyer-Marcotty P et al (2019) Reconstruction of the temporomandibular joint: a comparison between prefabricated and customized alloplastic prosthetic total joint systems. Int J Oral Maxillofac Surg 48(8):1066–1071. https://doi.org/10.1016/j.ijom.2019.02.002
7. Gerbino G, Zavattero E, Bosco G et al (2017) Temporomandibular joint reconstruction with stock and custom-made devices: indications and results of a 14-year experience. J Cranio-Maxillofac Surg 45(10):1710–1715. https://doi.org/10.1016/j.jcms.2017.07.011
8. Liu S, Shin YC (2019) Additive manufacturing of Ti6Al4V alloy: a review. Mater Des 164:107552. https://doi.org/10.1016/j.matdes.2018.107552
9. Javaid M, Haleem A (2018) Additive manufacturing applications in orthopaedics: a review. J Clin Orthop Trauma 9(3):202–206. https://doi.org/10.1016/j.jcot.2018.04.008
10. Edwards P, Ramulu M (2014) Fatigue performance evaluation of selective laser melted Ti-6Al-4V. Mater Sci Eng A 598:327–337. https://doi.org/10.1016/j.msea.2014.01.041
11. Abel EW, Hilgers A, McLoughlin PM (2015) Finite element analysis of a condylar support prosthesis to replace the temporomandibular joint. Br J Oral Maxillofac Surg 53(4):352–357. https://doi.org/10.1016/j.bjoms.2015.01.016
12. Ramos A, Gonzalez-Perez LM, Infante-Cossio P et al (2019) Ex-vivo and in vitro validation of an innovative mandibular condyle implant concept. J Cranio-Maxillofacial Surg 47(1):112–119. https://doi.org/10.1016/j.jcms.2018.11.010
13. Ramos A, Mesnard M (2016) A new condyle implant design concept for an alloplastic temporomandibular joint in bone resorption cases. J Cranio-Maxillofacial Surg 44(10):1670–1677. https://doi.org/10.1016/j.jcms.2016.07.024
14. Zheng J, Chen X, Jiang W et al (2019) An innovative total temporomandibular joint prosthesis with customized design and 3D printing additive fabrication: a prospective clinical study. J Transl Med 17(1):1–10. https://doi.org/10.1186/s12967-018-1759-1
15. Pinheiro M, Willaert R, Khan A et al (2021) Biomechanical evaluation of the human mandible after temporomandibular joint replacement under different biting conditions. Sci Rep 11:14034. https://doi.org/10.1038/s41598-021-93564-3
16. Gröning F, Liu J, Fagan MJ et al (2009) Validating a voxel-based finite element model of a human mandible using digital speckle pattern interferometry. J Biomech 42(9):1224–1229. https://doi.org/10.1016/j.jbiomech.2009.03.025
17. van Eijden TMGJ (2000) Biomechanics of the mandible. Crit Rev oral Biol Med 11(1):123–136
18. Korioth TW, Hannam AG (1994) Deformation of the human mandible during simulated tooth clenching. J Dent Res 73(1):56–66. https://doi.org/10.1177/00220345940730010801
19. Vanmeensel K, Lietaert K, Vrancken B et al (2018) Additively manufactured metals for medical applications. In: Zhang J, Jung YG (eds) Additive manufacturing—materials, processes, quantifications and applications, pp 261–309. https://doi.org/10.1016/B978-0-12-812155-9.00008-6
20. Ratner B, Hoffman A, Schoen F et al (2012) Biomaterials science: an introduction to materials in medicine, 3rd edn. Academic Press
21. Murphy W, Black J, Hastings G (2016) Handbook of biomaterial properties, 2nd edn. Springer, New York
22. Zhou ZR, Yu HY, Zheng J et al (2013) Dental biotribology, 1st edn. Springer, New York
23. Chern AH, Nandwana P, Yuan T et al (2019) A review on the fatigue behavior of Ti-6Al-4V fabricated by electron beam melting additive manufacturing. Int J Fatigue 119:173–184. https://doi.org/10.1016/j.ijfatigue.2018.09.022
24. Sam Froes FH, Qian M (2018) Titanium in medical and dental applications, 1st edn. Woodhead Publishing Duxford
25. Li P, Warner DH, Fatemi A et al (2016) Critical assessment of the fatigue performance of additively manufactured Ti-6Al-4V and perspective for future research. Int J Fatigue 85:130–143. https://doi.org/10.1016/j.ijfatigue.2015.12.003
26. Eichmiller F, Tesk JA, Croarkin CM (2001) Mechanical properties of ultra high molecular weight polyethylene NIST reference material RM 8456. Soc Biomater 22(6):20899
27. Tanaka E, Sasaki A, Tahmina K et al (2001) Mechanical properties of human articular disk and its influence on TMJ loading studied with the finite element method. J Oral Rehab 28(3):273–279. https://doi.org/10.1111/j.1365-2842.2001.tb01677.x
28. Mori H, Horiuchi S, Nishimura S et al (2010) Three-dimensional finite element analysis of cartilaginous tissues in human temporomandibular joint during prolonged clenching. Arch Oral Biol 55(11):879–886. https://doi.org/10.1016/j.archoralbio.2010.07.011
29. Bergmann G, Bender A, Dymke J et al (2016) Standardized loads acting in hip implants. PLoS ONE 11(5):e0155612. https://doi.org/10.1371/journal.pone.0155612
30. Bergmann G, Bender A, Graichen F et al (2014) Standardized loads acting in knee implants. PLoS ONE 9(1):e86035. https://doi.org/10.1371/journal.pone.0086035
31. Nagasao T, Nakajima T, Kimura A et al (2005) The dynamic role of buttress reconstruction after maxillectomy. Plast Reconstr Surg 115(5):1328–1340. https://doi.org/10.1097/01.prs.0000156978.16358.1e
32. Van Loon JP, Otten E, Falkenstrom CH et al (1998) Loading of a unilateral temporomandibular joint prosthesis: a three-dimensional mathematical study. J Dent Res 77(11):1939–1947. https://doi.org/10.1177/00220345980770111201
33. Choy SY, Sun CN, Leong KF et al (2017) Compressive properties of Ti-6Al-4V lattice structures fabricated by selective laser melting: design, orientation and density. Addit Manuf 16:213–224. https://doi.org/10.1016/j.addma.2017.06.012
34. Li SJ, Murr LE, Cheng XY et al (2012) Compression fatigue behavior of Ti-6Al-4V mesh arrays fabricated by electron beam melting. Acta Mater 60(3):793–802. https://doi.org/10.1016/j.actamat.2011.10.051
35. Waymel RF, Chew HB, Lambros J (2019) Loading orientation effects on the strength anisotropy of additively-manufactured Ti-6Al-4V alloys under dynamic compression. Exp Mech 59(6):829–841. https://doi.org/10.1007/s11340-019-00506-2
36. Budynas R (2014) Shigley's mechanical engineering design. McGraw-Hill Higher Education
37. Pinheiro M, Ma X, Fagan MJ et al (2019) A 3D cephalometric protocol for the accurate quantification of the craniofacial symmetry and facial growth. J Biol Eng 13:42. https://doi.org/10.1186/s13036-019-0171-6
38. Bendsoe MP, Sigmund O (2003) Topology optimization—theory, methods, and applications, 2nd edn. Springer
39. Tanlak N, Frederik De Lange D, Van Paepegem W (2017) Numerical prediction of the printable density range of lattice structures for

additive manufacturing. Mater Des 133:549–558. https://doi.org/10.1016/j.matdes.2017.08.007
40. Larsson R (2016) Methodology for topology and shape optimization: application to a rear lower control arm. Chalmers University of Technology Gothenburg
41. Frost HM (2003) Bone's mechanostat: a 2003 update. Anat Rec A Discov Mol Cell Evol Biol 275(2):1081–1101. https://doi.org/10.1002/ar.a.10119
42. Ichim I, Kieser JA, Swain MV (2007) Functional significance of strain distribution in the human mandible under masticatory load: numerical predictions. Arch Oral Biol 52(5):465–473. https://doi.org/10.1016/j.archoralbio.2006.10.020
43. Gröning F, Fagan MJ, O'higgins P (2013) Comparing the distribution of strains with the distribution of bone tissue in a human mandible: a finite element study. Anat Rec 296(1):9–18. https://doi.org/10.1002/ar.22597
44. Linden RWA (1998) Mastication. In Linden RWA (ed) The scientific basis of eating: taste and smell, salivation, mastication and swallowing, and their dysfunctions, 1st edn. Karger Medical and Scientific Publishers, pp 76–121
45. Roldan SI, Restrepo LG, Isaza JF et al (2016) Are maximum bite forces of subjects 7 to 17 years of age related to malocclusion? Angle Orthod 86(3):456–461. https://doi.org/10.2319/051315-323.1
46. Ferrario VF, Sforza C, Serrao G et al (2004) Single tooth bite forces in healthy young adults. J Oral Rehabil 31(1):18–22. https://doi.org/10.1046/j.0305-182X.2003.01179.x
47. Bergmann G (2010) Realistic loads for testing hip implants. Biomed Mater Eng 20(2):65–75. https://doi.org/10.3233/BME-2010-0616
48. Browne M, Langley RS, Gregson PJ (1999) Reliability theory for load bearing biomedical implants. Biomaterials 20(14):1285–1292. https://doi.org/10.1016/s0142-9612(99)00027-7
49. Cheng YC, Jiang CP, Lin DH (2019) Finite element based optimization design for a one-piece zirconia ceramic dental implant under dynamic loading and fatigue life validation. Struct Multidiscip Optim 59(3):835–849. https://doi.org/10.1007/s00158-018-2104-2
50. Xu L, Fan S, Cai B et al (2017) Influence of sustained submaximal clenching fatigue test on electromyographic activity and maximum voluntary bite forces in healthy subjects and patients with temporomandibular disorders. J Oral Rehab 44(5):340–346. https://doi.org/10.1111/joor.12497
51. Ackland D, Robinson D, Lee PVS et al (2018) Design and clinical outcome of a novel 3D-printed prosthetic joint replacement for the human temporomandibular joint. Clin Biomech 56:52–60. https://doi.org/10.1016/j.clinbiomech.2018.05.006
52. Mesnard M, Ramos A, Simoes JA (2014) Influences of implant condyle geometry on bone and screw strains in a temporomandibular implant. J Cranio-Maxillofacial Surg 42(3):194–200. https://doi.org/10.1016/j.jcms.2013.04.010
53. Al-Tamimi AA, Peach C, Fernandes PR et al (2017) Topology optimization to reduce the stress shielding effect for orthopedic applications. Procedia CIRP 65:202–206. https://doi.org/10.1016/j.procir.2017.04.032
54. Guo LX, Yin JY (2019) Finite element analysis and design of an interspinous device using topology optimization. Med Biol Eng Comput 57(1):89–98. https://doi.org/10.1007/s11517-018-1838-8
55. Iqbal T, Wang L, Li DC et al (2019) A general multi-objective topology optimization methodology developed for customized design of pelvic prostheses. Med Eng Phys 69:8–16. https://doi.org/10.1016/j.medengphy.2019.06.008